ARTICLE

Mutations in the NHEJ Component *XRCC4* Cause Primordial Dwarfism

Jennie E. Murray,[1,13] Mirjam van der Burg,[2,13] Hanna IJspeert,[2] Paula Carroll,[1] Qian Wu,[3] Takashi Ochi,[3] Andrea Leitch,[1] Edward S. Miller,[4] Boris Kysela,[5] Alireza Jawad,[2] Armand Bottani,[6] Francesco Brancati,[7] Marco Cappa,[8] Valerie Cormier-Daire,[9] Charu Deshpande,[10] Eissa A. Faqeih,[11] Gail E. Graham,[12] Emmanuelle Ranza,[6] Tom L. Blundell,[3] Andrew P. Jackson,[1,*] Grant S. Stewart,[4,*] and Louise S. Bicknell[1]

Non-homologous end joining (NHEJ) is a key cellular process ensuring genome integrity. Mutations in several components of the NHEJ pathway have been identified, often associated with severe combined immunodeficiency (SCID), consistent with the requirement for NHEJ during V(D)J recombination to ensure diversity of the adaptive immune system. In contrast, we have recently found that biallelic mutations in *LIG4* are a common cause of microcephalic primordial dwarfism (MPD), a phenotype characterized by prenatal-onset extreme global growth failure. Here we provide definitive molecular genetic evidence supported by biochemical, cellular, and immunological data for mutations in *XRCC4*, encoding the obligate binding partner of LIG4, causing MPD. We report the identification of biallelic mutations in *XRCC4* in five families. Biochemical and cellular studies demonstrate that these alterations substantially decrease XRCC4 protein levels leading to reduced cellular ligase IV activity. Consequently, NHEJ-dependent repair of ionizing-radiation-induced DNA double-strand breaks is compromised in XRCC4 cells. Similarly, immunoglobulin junctional diversification is impaired in cells. However, immunoglobulin levels are normal, and individuals lack overt signs of immunodeficiency. Additionally, in contrast to individuals with *LIG4* mutations, pancytopenia leading to bone marrow failure has not been observed. Hence, alterations that alter different NHEJ proteins give rise to a phenotypic spectrum, from SCID to extreme growth failure, with deficiencies in certain key components of this repair pathway predominantly exhibiting growth deficits, reflecting differential developmental requirements for NHEJ proteins to support growth and immune maturation.

Introduction

Microcephalic primordial dwarfism (MPD) encompasses a heterogeneous group of disorders, all characterized by extreme global growth failure. The cardinal features of MPD are in utero and postnatal growth retardation with significant microcephaly, with height and occipitofrontal circumference (OFC) at least 4 SD below the mean.[1,2] Clinically recognizable forms of MPD include MOPD I (MIM 210710) caused by mutations in the U12 minor spliceosomal component, *RNU4ATAC* (MIM 601428);[3,4] MOPD II (MIM 210720) due to mutations in *PCNT* (MIM 605925), encoding the centrosomal scaffold protein, pericentrin;[5,6] and defects in multiple components of the pre-replication complex resulting in Meier-Gorlin syndrome (MIM 224690, 613800, 613802, 613803, 613804).[7–9] A number of important DNA damage response genes have also been implicated in MPD, including *ATR* (MIM 601215), *ATRIP* (MIM 606605), and *RBBP8* (encoding CtIP) (MIM 604124),[10–12] which are associated with Seckel syndrome. However, it is still difficult to clinically categorize many individuals with MPD based solely on phenotype, with a syndromic diagnosis often not possible. A gene-based classification for diagnosis and subsequent management would be desirable, although at present this is not possible for a significant proportion of individuals for whom the molecular basis of their MPD has yet to be established.

Recently, we and others identified biallelic truncating mutations in *LIG4* (MIM 601837), which encodes the principal ligase involved in non-homologous end joining (NHEJ)-mediated DNA repair, in a large number of MPD-affected individuals[13,14] and also two Dubowitz-affected siblings,[15] establishing this as the second most common cause of MPD after *PCNT* mutations. LIG4 deficiency (MIM 606593) had previously been described for a range of phenotypes including severe combined immunodeficiency (SCID), microcephaly, and isolated radiation hypersensitivity/malignancy predisposition.[13,16–22]

The NHEJ pathway (reviewed in Chiruvella et al.[23] and Deriano and Roth[24]) is the primary cellular mechanism for template-independent repair of double-strand DNA

[1]MRC Human Genetics Unit, MRC Institute of Genetics and Molecular Medicine, University of Edinburgh, Edinburgh EH4 2XU, UK; [2]Department of Immunology, Erasmus MC, University Medical Center Rotterdam, 3015 Rotterdam, the Netherlands; [3]Department of Biochemistry, University of Cambridge, Cambridge CB2 1GA, UK; [4]School of Cancer Sciences, University of Birmingham, Birmingham B15 2TT, UK; [5]School of Clinical and Experimental Medicine, University of Birmingham, Birmingham B15 2TT, UK; [6]Department of Genetic Medicine, University Hospitals of Geneva, 1205 Geneva, Switzerland; [7]Department of Medical, Oral and Biotechnological Sciences, Gabriele D'Annunzio University of Chieti-Pescara, 66100 Chieti, Italy; [8]Endocrinology and Diabetes Unit, IRCCS Bambino Gesù Children's Hospital, 00165 Rome, Italy; [9]Department of Genetics, INSERM UMR 1163, Université Paris Descartes-Sorbonne Paris Cité, Institut Imagine, Hôpital Necker Enfants Malades, Assistance Publique-Hôpitaux de Paris, Paris 75015, France; [10]Department of Genetics, Guy's Hospital, Guy's and St Thomas' NHS Foundation Trust, London SE1 9RT, UK; [11]Children's Specialist Hospital, King Fahad Medical City, Riyadh 11525, Saudi Arabia; [12]Department of Genetics, Children's Hospital of Eastern Ontario, Ottawa, ON K1H 8L1, Canada
[13]These authors contributed equally to this work
*Correspondence: andrew.jackson@igmm.ed.ac.uk (A.P.J.), g.s.stewart@bham.ac.uk (G.S.S.)
http://dx.doi.org/10.1016/j.ajhg.2015.01.013.

breaks (DSBs). Free DNA ends are rapidly bound by the Ku70-Ku80 heterodimer, which recruits and activates DNA-PK_{CS} and Artemis, the latter of which is required to cleave damaged DNA overhangs prior to infilling by polymerases μ and λ. Finally, ligation is performed by the XRCC4-XLF-LIG4 complex. XRCC4 and XLF are thought to act in concert to form a filament that wraps around the DNA ends, bridging the gap and acting as a stabilizer for LIG4 to complete ligation.[25] In addition to repairing spontaneous and ionizing-radiation-induced breaks, the NHEJ pathway plays an essential role in V(D)J recombination to ensure a diverse repertoire of T and B cells.[26] After the cleavage of DNA at the recombination signal sites by RAG1 and RAG2, the NHEJ components stabilize the free DNA ends and permit random deletion of nucleotides by nucleases and random insertion of non-templated nucleotides by terminal deoxytransferase (TdT), before final ligation by XRCC4-XLF-LIG4.

Mutations have been described in many components of the NHEJ pathway,[27] including *DCLRE1C* (encoding Artemis [MIM 605988]),[27] *PRKDC* (encoding DNA-PK_{CS} [MIM 600899]),[28] and *NHEJ1* (encoding XLF [MIM 611290]),[29–31] associated with SCID with or without associated microcephaly and variable stature. Given the association of *LIG4* with MPD, *XRCC4* (MIM 194363) was also recently suggested as a candidate gene in which a mutation might cause MPD,[32] after identification of a rare missense variant in an exome-sequencing dataset of a single MPD-affected individual. However, given additional homozygous rare variants and without assessment of the functional consequences of this variant on protein function, the authors were not able to categorically assign pathogenicity to this variant.

Here, we report the identification of pathogenic mutations in *XRCC4* in multiple MPD-affected individuals, providing definitive molecular genetic evidence that mutations in *XRCC4* cause a human disease. We characterize in detail the cellular, immunological, and phenotypic consequences of these mutations, establishing that *XRCC4* mutations primarily result in a MPD phenotype without overt immunodeficiency.

Material and Methods

Family Ascertainment and Mutation Identification

Recruitment, exome sequencing, and variant validation were performed as described previously.[14] Informed consent was obtained from all participating families, and the studies were approved the Scottish Multicenter Research Ethics Committee (04:MRE00/19). Parents provided written consent for the publication of photographs of the affected individuals. Z-scores (standard deviations) were calculated by the LMS method on 1990 British Growth reference data.[33] Cohort resequencing was performed by Ion AmpliSeq multiplex PCR (Life Technologies). Primers were designed to amplify all *XRCC4* coding exons with 25 bp of flanking intronic sequence and PCR amplification performed in1/6^{th} reaction volumes for each of three primer pools with 5 ng of human DNA. After pooling of all amplicons per individual, Ion Xpress barcoding was performed in 1/2 reaction volumes, quantified by BioAnalyser high sensitivity chips and equal amounts of pooled amplification products. Sequencing was performed with the Ion P1 200 Sequencing Kit on the Ion Proton sequencing platform (Life Technologies). Variants were called with Torrent Suite software. Variant filtering was performed as per exome analysis[34] and sequence reads visually inspected by IGV.[35] All variants were confirmed by capillary sequencing; in individuals in whom a single heterozygous deleterious variant was identified by NGS, the entire coding sequence of *XRCC4* was resequenced by capillary sequencing (due to the higher false negative rate for mutation identification around homopolymer tracts by Ion sequencing technology, to ensure a second mutation hadn't been misclassified in the initial high-throughput sequencing). PCR conditions and primer sequences are available upon request.

Construct Design and Purification

XRCC4 was amplified from pET30XRCC4[36] and inserted between *Nco*I and *Bam*HI sites pHAT5 vector[37] to fuse a hexahistidine tag at the C terminus of XRCC4 (pHAT5XRCC4). Plasmids expressing $XRCC4^{p.Trp43Arg}$ with and without LIG4 were created from pHAT5XRCC4 and pRSFDuet-*lig4*-His[6]-xrcc4,[38] respectively, via site-directed mutagenesis. XRCC4 and $XRCC4^{p.Trp43Arg}$ were purified through affinity chromatography (5 ml HisTrap HP column [GE Healthcare]), anion-exchange chromatography (5 ml HiTrap Q HP column [GE Healthcare]), and finally size-exclusion column (Superdex 200 10/300 GL [GE Healthcare]). The final buffer for the XRCC4 constructs is 20 mM Tris-HCl (pH 8.0), 300 mM NaCl, 5% (v/v) glycerol, and 5 mM DTT. $XRCC4^{p.Trp43Arg}$/LIG4 was purified in the same manner as the wild-type.[38] The SDS-PAGE gel (Figure 2C) was analyzed by mass spectrometry by Dr. Len Packman in the PNAC facility, Department of Biochemistry, University of Cambridge to confirm that purified proteins visualized were LIG4 and $XRCC4^{p.Trp43Arg}$.

Clonogenic Survival Assay

Clonogenic survival assays with primary skin fibroblasts were performed as described previously.[22] LIG4 cells were derived from F10, reported by Murray et al.[14]; Artemis cells are human-derived fibroblasts from Lee et al.[40] In brief, primary skin fibroblasts in exponential growth were trypsinized, and 500–2,000 cells (5,000–80,000 cells for the highest doses) were seeded into 10 cm plastic dishes (2 dishes per dose) and irradiated at room temperature at a dose of approximately 1 Gy/min. After 12–14 days, the cells were rinsed with 0.9% NaCl and stained with 0.25% methylene blue for survival assessment.

Immunofluorescence

Cells were seeded onto coverslips, irradiated, fixed in ice-cold 3.6% PFA-PBS for 10 min, permeabilized in ice-cold extraction buffer (10 mM PIPES, 20 mM NaCl, 3 mM $MgCl_2$, 300 mM sucrose, 0.5% Triton X-100) for 5 min, and then blocked in 10% FCS for 1 hr at room temperature. Asynchronously growing cells were stained with an anti-γ-H2AX antibody (Millipore) only, whereas G1-arrested cells were stained with an anti-γ-H2AX antibody in combination with antibody to Cyclin A (Santa Cruz Biotechnology). Micronuclei were detected by DAPI staining. Secondary antibodies used were Alexa Fluor-594 goat anti-mouse IgG and Alexa Fluor-488 goat anti-rabbit IgG (Invitrogen). Fluorescence images were taken with a Nikon E600 Eclipse microscope

equipped with a 60× oil lens, and images were acquired and analyzed with Volocity Software v.4.1 (Improvision). The number of γ-H2AX foci per cell was quantified for a minimum of 500 cells per time point. In the case of the γ-H2AX foci quantification in G1-arrested cells, γ-H2AX foci were counted only in cells negative for Cyclin A staining.

Antibodies and Western Immunoblotting

Whole-cell extracts were obtained by sonication in UTB buffer (8 M Urea, 50 mM Tris [pH 7.5], 150 mM β-mercaptoethanol) and centrifugation to remove insoluble debris. The following antibodies were used: DNA-PK_{CS} (Santa Cruz Biotechnology); phospho-DNA-PK_{CS} Ser-2056, DNA Ligase IV, XRCC4, and XLF (Abcam); phospho-KAP1 Ser824 and KAP1 (Bethyl); Ku80, H2A, and γ-H2AX (Millipore), with secondary antibodies: swine anti-rabbit IgG-HRP and goat anti-mouse IgG-HRP (Dako).

DNA DSB Labeling

All cell lines were routinely maintained as monolayers at 37°C. In DNA DSB induction/rejoining experiments, 1–2 × 10^6 cells were seeded in 75 cm^2 flasks 4 days prior to irradiation. 24 hr after seeding, the exponentially growing cells were radioactively labeled by media replacement with fresh, complete MEM supplemented with 0.02 μCi/ml ^{14}C-thymidine (DuPont, 59 mCi/mmol) for 48–50 hr. Typically, values between 0.02 and 0.08 dpm per cell were found at the end of the labeling period.

Pulse-Field Gel Electrophoresis

Conditions used are modified from Kysela et al.[41] After 48–50 hr incubation, cells in stationary phase were released for a 2 hr chase period. Cells were mixed gently with an equal volume of a 1% solution of low-melting-point agarose (BRL) in PBS at a final density of 2.5–3.0 × 10^6 cells/ml to form agarose plugs. After solidification, plugs were irradiated in air on ice with 240 kVp X-rays at a dose rate of 2.9 Gy/min. Immediately after irradiation, the cells were lysed on ice with 3 volumes of lysis solution (0.5 M EDTA, 1% N-lauroylsarcosine, 1 mg/ml proteinase K) and incubating at 50° for 40 hr. In order to investigate DNA DSB repair, the irradiated inserts (together with unirradiated controls) were placed into 7 ml of pre-warmed complete MEM in culture dishes, incubated under normal growth conditions for various time intervals, and then lysed as described above. After lysis, DNA samples in agarose inserts were extensively washed 5 times against 100 volumes of TE buffer to avoid any remaining proteinase K and detergent contamination.

Agarose gels (0.8%, BRL ultraPURE) were cast in 0.5× TBE buffer (1× TBE: 90 mM Tris base, 90 mM boric acid, and 2.5 mM EDTA). Electrophoresis conditions used were: initial switching time, 30 min; final switching time, 30 min; running time, 48 hr; voltage, 1.5V/cm; angle, 120°; temperature, 14°C; on a CHEF-DR III apparatus (BIORAD). Gels were analyzed with STORM Phosphorimager.

IGH Repertoire Analysis

VH-JH junctions were amplified from peripheral blood mononuclear cells in a multiplex PCR with the VH1-6 FR1 and JH consensus BIOMED-2 primers.[42] The primers were adapted for 454 sequencing by adding the forward A or reverse B adaptor, the "TCAG" key, and multiplex identifier (MID) adaptor. PCR products were purified by gel extraction (QIAGEN) and Agencourt AMPure XP beads (Beckman Coulter). Subsequently, the PCR concentration was measured with the Quant-it Picogreen dsDNA assay (Invitrogen). The purified PCR products were sequenced on the 454 GS junior instrument according the manufacturer's recommendations, using the GS junior Titanium emPCR kit (Lib-A), sequencing kit, and PicoTiterPlate kit (454 Life Sciences, Roche). Using the CLC genomic workbench software, the samples were separated based on their MID sequence and trimmed and reads with a quality score below 0.05 and below 250 bp were discarded. The reads were uploaded to IMGT HighV-Quest.[43] Subsequently these output files were uploaded to the custom Galaxy platform.[44–46] Further processing was done in the 'R' programing language[47] to generate the tabular outputs.

In Vitro V(D)J Recombination

XR1 cells (*XRCC4*-deficient Chinese hamster ovary cells) were transfected with a recombination substrate (pDVG93) containing two recombination signal sequences (RSS) in inverted orientation, *RAG1* and *RAG2* expression constructs, and pCDNA containing either WT or *XRCC4* mutation expression constructs. After 48 hr, the cells were harvested and extrachromosomal DNA was isolated. Upon recombination, the sequence between the two RSS is inverted, which could be detected by qRT-PCR. The level of recombination activity of wild-type XRCC4 was set at 100%.

Results

Identification of *XRCC4* Mutations in Six MPD-Affected Individuals

After our recent report of *LIG4* mutations in 11 individuals,[14] we identified further compound heterozygous mutations in *LIG4* by exome sequencing in dizygotic twins with MPD (Table S1). In addition to the common previously reported p.Arg814* termination, the two siblings were compound heterozygous for the missense mutation c.2321T>C (p.Leu774Pro) (RefSeq accession number NM_002312.3). Leu774 lies within the XRCC4 binding motif and is conserved between humans and yeasts (Figure S1). The location of the substitution led us to hypothesize that the interaction between LIG4 and XRCC4 might be of particular relevance to the growth phenotype.

Additionally, analysis of exome sequencing for rare, deleterious recessive variants in a large cohort of MPD-affected individuals identified a homozygous missense variant in *XRCC4* in a Saudi Arabian individual (P1) with extreme microcephaly (−8.3 SD) and short stature (−4.7 SD). This mutation, c.127T>C (p.Trp43Arg) (RefSeq NM_022550.2), was confirmed by capillary sequencing and segregated appropriately within the family. The allele frequency for this variant was 3.3 × 10^{-5} in control populations, with no homozygotes reported (ExAC Consortium). The deleterious prediction by SnpEff[48] in combination with the rare allele frequency suggested that mutations in *XRCC4* represent a previously uncharacterized cause of MPD.

Given these two lines of evidence, the entire coding region of *XRCC4* was resequenced in our cohort of MPD-affected individuals (n = 208) via AmpliSeq multiplex PCR/Ion Proton NGS sequencing. This resulted in identification of five additional individuals from four families with biallelic mutations in *XRCC4* (Table 1, Figure 1). All

Table 1. Mutations in *XRCC4* in MPD-Affected Individuals

Pt	Nucleotide Mutations	Amino Acid Alterations	Sex	Country of Origin
P1	c.127T>C (homozygous)	p.Trp43Arg	M	Saudi Arabia
P2	c.481C>T + c.673C>T	p.Arg161* + p.Arg225*	M	Morocco
P3-1	c.25delC + c.823C>T	p.His9Thrfs*8 + p.Arg275*	M	Italy
P3-2	c.25delC + c.823C>T	p.His9Thrfs*8 + p.Arg275*	M	Italy
P4	c.25delC + c.823C>T	p.His9Thrfs*8 + p.Arg275*	M	France
P5	c.25delC + c.−10−1G>T	p.His9Thrfs*8 + (splicing)	M	UK

RefSeq NM_022550.2. All parents were sequenced and mutations segregated appropriately.

mutations identified were validated by capillary sequencing in affected individuals, and segregation was confirmed in parents.

Individuals with *XRCC4* Mutations Exhibit Severe Pre- and Postnatal Growth Failure

Growth measurements in all individuals (Figure 1A, Table 2) demonstrated significant reduction in both head and body size at birth (median OFC −3.59 ± 1.19 SD; length −4.94 ± 1.75 SD; weight −3.14 ± 0.64 SD). Postnatally, affected individuals developed extreme microcephaly (median −8.15 ± 1.93 SD) along with significant reduction in height (−4.6 ± 2.02 SD), similar to those we previously reported for individuals with *LIG4* mutations.[14] Additionally, individuals with XRCC4-MPD exhibited facial similarities, including fine sparse hair, small chin, and broad nasal tip (Figure 1B). Developmental delay was present in only some, and no recurrent developmental malformations were apparent. No malignancies were reported and, importantly, there was no clinical suspicion of immunodeficiency in these individuals.

XRCC4 Mutations Markedly Reduce Cellular Levels of XRCC4 and LIG4

We predicted that prematurely truncating *XRCC4* mutations were likely to be functionally deleterious by reducing protein levels via nonsense-mediated decay (Figure 2A). For the substitution p.Trp43Arg, its conservation in vertebrates suggests that it would also substantially impact function (Figure 2B). Furthermore, structural analysis suggested that substitution of this hydrophic residue (Trp43) with a positively charged arginine would lead to the destabilization of the XRCC4 head domain. Trp43 is a part of a hydrophobic core formed by Leu36, Asp38, Ser41, Phe88, Lys90, Leu113, and Lys115 (Figure 2C), and the substitution to arginine was predicted to cause a distortion of two layers of β sheets, disrupting the buried hydrophobic core, as well as affecting the helix-turn-helix motif in the head domain of XRCC4. Additionally, structure-based computational analysis of the p.Trp43Arg substitution via DUET[49] indicated that the substitution destabilizes the structure of XRCC4.

To address these structural predictions, we expressed and purified recombinant XRCC4^{WT} and XRCC4$^{p.Trp43Arg}$ from *E. coli*. Significantly, in contrast to wild-type XRCC4, the p.Trp43Arg substitution greatly reduced protein solubility, with the majority of the full-length protein residing in insoluble fractions of the bacterial extract. Despite this, we were able to purify some full-length XRCC4$^{p.Trp43Arg}$ protein. However, this was more prone to degradation (Figure 2D), either when expressed by itself or in combination with LIG4. Furthermore, although the circular dichroism (CD) spectrum of the XRCC4$^{p.Trp43Arg}$ form indicated that the protein is folded, it differed from wild-type (Figure S2). Nevertheless, because in vitro ligation assays using XRCC4$^{p.Trp43Arg}$ recombinant protein in conjunction with either blunt or cohesive DNA ends did not detect any significant reduction in ligation efficiency (Figure S3), we concluded that the p.Trp43Arg substitution more likely affects protein stability rather than directly affecting XRCC4 function.

Because human-derived primary fibroblasts containing the p.Trp43Arg substitution were available from P1, we next performed immunoblotting to assess cellular levels of NHEJ components (Figure 2E). Protein levels of XRCC4 were strongly reduced in P1 cells, in keeping with our biochemical analysis. Furthermore, XLF and particularly LIG4, which form a complex with XRCC4, were also reduced, indicating that the reduction in XRCC4 affects stability of this whole complex. Likewise, a similar decrease of XRCC4/LIG4/XLF was also seen in *LIG4* human cells (derived from F10, reported in Murray et al.[14]). Other components of the NHEJ machinery (Ku80 and DNA-PK$_{CS}$) were not decreased in either LIG4 or XRCC4 cells, in keeping with their role upstream of the XRCC4/LIG4/XLF complex.

Primary fibroblasts were also available from individual P5. Here an early truncating mutation was present (c.25delC [p.His9Thrfs8*]) in conjunction with an essential splice acceptor mutation in exon 2 (c.−10−1G>T). RT-PCR identified an aberrant splicing product (Figure S4) that results in loss of exon 2 (containing the translation initiation codon) from a proportion of transcripts. This, in conjunction with the early truncating mutation, would be expected to lead to marked reduction in protein levels, and indeed immunoblotting of protein extracts from P5 fibroblasts detected markedly reduced XRCC4 (and LIG4) levels (Figure 2E).

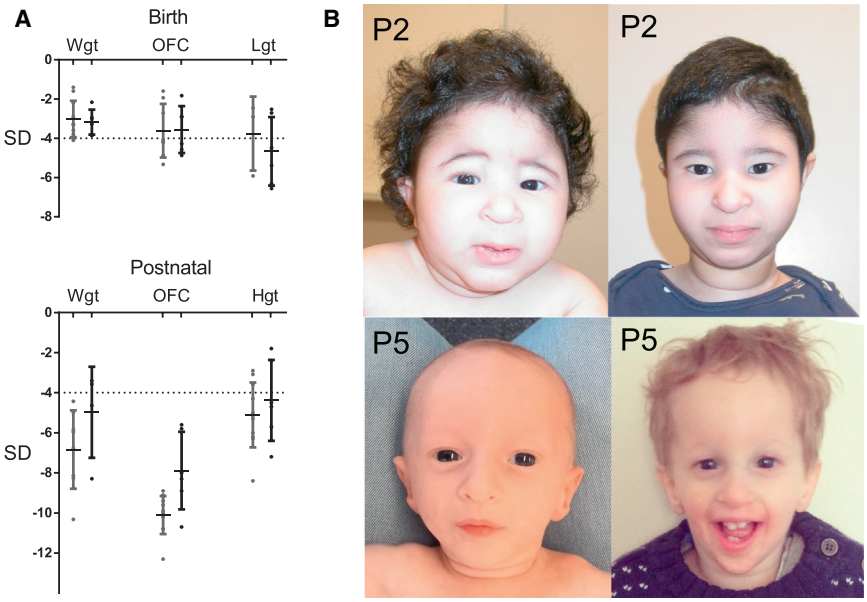

Figure 1. Mutations in *XRCC4* Result in Prenatal-Onset Growth Failure with Disproportionate Microcephaly

(A) Growth is delayed both pre- and post-natally; individuals with XRCC4 alterations (black) have similar growth parameters to those seen in individuals with LIG4 alterations (gray).[14] Data plotted for six individuals with biallelic missense or truncating mutations in *XRCC4*. Mean ± SD. Abbreviations are as follows: OFC, occipital-frontal circumference; Wgt, weight; Lgt, length; Hgt, height.

(B) Facial features of individuals with mutations in *XRCC4*. P2 aged 11 months (left) and 4 years (right); P5 aged 5 months (left) and 21 months (right).

From these cellular studies, we concluded that *XRCC4* mutations lead to substantial loss of both XRCC4 and LIG4 from cells, which would be predicted to result in a significantly reduced activity of the ligase IV complex, impairing NHEJ. We therefore next examined NHEJ activity in these cells.

Cells with *XRCC4* Mutations Have Elevated Sensitivity to Ionizing Radiation due to Impaired NHEJ

NHEJ-deficient cells have increased sensitivity to ionizing radiation (IR).[27] Therefore, we assessed XRCC4 fibroblast viability after IR in a clonogenic survival assay. After irradiation, *XRCC4*-mutated cells exhibited impaired survival (Figure 3A) with hypersensitivity to IR comparable to cells from published Artemis- and LIG4-altered individuals.[13,50] To further characterize the cellular response to IR in these cells in more detail, we monitored the resolution of γ-H2AX foci by immunofluorescence as a measure of their capacity to repair DSBs. After irradiation, equal numbers of foci were detected in XRCC4 and control cells; however, at 24 hr after irradiation, 99.4% of P1 and 62.3% of P5 asynchronous cells had >5 γ-H2AX foci compared to 9.2% control cells ($p < 0.0001$), indicating that *XRCC4* (and *LIG4*) mutations disrupted the ability of the cell to resolve DNA damage induced by IR (Figure 3B). To confirm that this was the consequence of defective NHEJ, cells were synchronized in G1 by contact inhibition and followed over a time course of 24 hr to examine the kinetics of DSB repair (Figures S5 and S6). XRCC4 fibroblasts again failed to resolve DNA breaks at 24 hr after IR ($p < 0.001$) (Figures 3Bii and S6). This observation was confirmed by immunoblotting, which also showed persistent activation of the DNA damage response in these cells in response to low-dose gamma radiation (Figure 3E). This is suggestive of defective NHEJ, because homologous recombination is not active in this cell cycle stage. Consistent with this, pre-treatment of the human-derived fibroblasts with a DNA-PK inhibitor prior to irradiation did not exacerbate the defect in resolving γ-H2AX foci (Figure S5).

To investigate DSB repair kinetics in cells more directly, we performed pulse-field gel electrophoresis (PFGE) (Figure 3C). After irradiation, the initial levels of DSBs were comparable between *XRCC4*-mutated and control cells (Figure 3Ci). However, over a 24 hr time course, almost 95% of DNA breaks detected by PFGE were resolved in control cells compared to only 42% of *XRCC4*-mutated cells ($p = 4 \times 10^{-8}$, t test, $n = 5$ experiments). In keeping with this, we observed increased numbers of micronuclei in *XRCC4*-mutated cells, most likely due to a failure to repair DSBs (Figure 3D, $p < 0.05$, ANOVA, $n = 3$ experiments).

We therefore concluded that *XRCC4* mutations lead to significant impairment of DSB break repair in cells.

Clinical Immunological Parameters Are Normal in Most Individuals with *XRCC4* Mutations

No increased susceptibility to infection was reported by clinicians caring for XRCC4-MPD-affected individuals. However, given the immunodeficiency documented in individuals with mutations in other NHEJ genes,[40] due to either T/B cell depletion as the consequence of failed V(D)J recombination or progressive pancytopenia and bone marrow failure in LIG4-MPD-affected individuals,[13,14] we performed detailed immunological and hematological investigations.

Strikingly, for the majority of individuals, there was no evidence of immunodeficiency or bone marrow failure, with blood cell counts, T cell and B cell subsets, and immunoglobulin (Ig) levels all within the normal ranges (Table 3). An isolated lymphopenia was evident in P1, affecting all T cell and B cell subsets, and a borderline leukopenia was recorded in P3-1, without deficits in T/B cell subsets. For P1 (with the p.Trp43Arg substitution), the reduction in lymphocyte number was chronic and nonprogressive on

Table 2. Phenotypic Characteristics of Individuals with *XRCC4* Mutations

	Birth						Postnatal					Developmental Delay	Additional Clinical Features
Pt	Gest (weeks)	Weight (kg)	SD[a]	OFC (cm)	SD	Length (cm)	SD	Age at Exam	OFC (cm)	SD	Height (cm)	SD		
P1	40	1.8	−3.87	29	−4.87	46	−2.52	3 years 1 month	39.8	−8.3	78.7	−4.7	moderate	none reported
P2	32	0.903	−3.27	24	−4.57	34	−6.32[b]	2 years 9 months	36.4	−10.7	73.4	−5.7	severe	gastrostomy, ectopic kidney, small bilateral kidneys, chronic lung disease
P3-1	36	1.55	−3	29	−2.9	39	−4.49	8 years 4 months	46	−5.6	130	−2.4	none	none reported
P3-2	37	1.72	−2.95	31	−1.83	38	−5.38	4 years	40.5	−8.0	84	−4.5	none	none reported
P4	NA	2.2	−2.16	28.5	−4.28	44	−2.71	9 years	45	−5.8	123	−1.8[c]	moderate	unilateral renal agenesis, cryptorchidism
P5	36	1.25	−3.83	29	−2.9	35	−6.56	5 months	33	−8.9	49.7	−7.2	unknown	eczema

[a]Adjusted for gestation
[b]Gestation of 34 weeks used in adjustment
[c]From −4 to −2 after growth hormone treatment.

repeated measurements, with lymphocyte count being 20% of mean reference range at 3 and 6 years (Table S3).

Further, extended assessment of T cell and B cell subsets was performed on three of the individuals by FACS (Table S2). Normal values were demonstrated for all subsets analyzed in P3-1 and P3-2; and for P1, naive, effector, and central/memory B cell and T cell subsets were all present, albeit at reduced levels. Additionally, levels of IgG and IgA were within the normal range for P1, indicating that despite class switching being dependent on NHEJ, XRCC4 deficiency has not hampered switching from IgM. Furthermore, P1 demonstrated normal responses to vaccines (Table S4).

We therefore concluded that our XRCC4 cohort had functional immune systems. Depletion of lymphocytes in P1 could be accounted for by impaired V(D)J recombination depleting T/B cell pools, so we next examined XRCC4 deficiency on V(D)J recombination at a molecular level.

Immune Receptor Junction Diversity Is Perturbed in Individuals with *XRCC4* Mutations

To assess the molecular impact of XRCC4 deficiency on V(D)J recombination, we undertook deep sequencing across V(D)J junctions from peripheral blood lymphocytes. By using 454 sequencing, we defined the repertoire of functional *IGH* gene rearrangements in both control and XRCC4 cells, quantifying the number of unique junction sequences generated, as well as characteristics such as nucleotide deletions, random non-templated nucleotide (N) insertions, and palindromic (P) nucleotides caused by asymmetric hairpin opening (Figure 4). Substantial junctional diversity was present in XRCC4 cells, with large numbers of unique productive *IGH* sequences being detected, and in keeping with adequate functioning of adaptive immunity in these individuals. Furthermore, there were no quantitative differences in nucleotide deletions or palindromic nucleotides from controls. However, there were significant reductions in the total number of random nucleotides inserted in V(D)J junctions of individuals with *XRCC4* mutations ($p < 0.008$). Given that nucleotide insertion is performed by the DNA polymerase TdT and in vitro the action of TdT is mediated by NHEJ components Ku80 and XRCC4,[51] this therefore provided in vivo validation for the role of XRCC4 in this aspect of V(D)J recombination.

Finally, we comprehensively assessed the effect of all the mutations identified on V(D)J recombination in an in vitro overexpression recombination assay (Figure 4B). As expected from our cellular studies, the point substitution p.Trp43Arg resulted in impaired, but not completely abrogated, V(D)J recombination ($p = 0.004$, t test). All other individuals were compound heterozygous for two truncating mutations; for every individual at least one segregating mutation (encoding p.Arg275* or p.Arg225*) had residual functionality in this assay. Hence, although these mutations are prematurely truncating and therefore subjected to nonsense-mediated decay, a small fraction might escape, producing truncated protein that is functional for V(D)J recombination within the cells. The embryonic

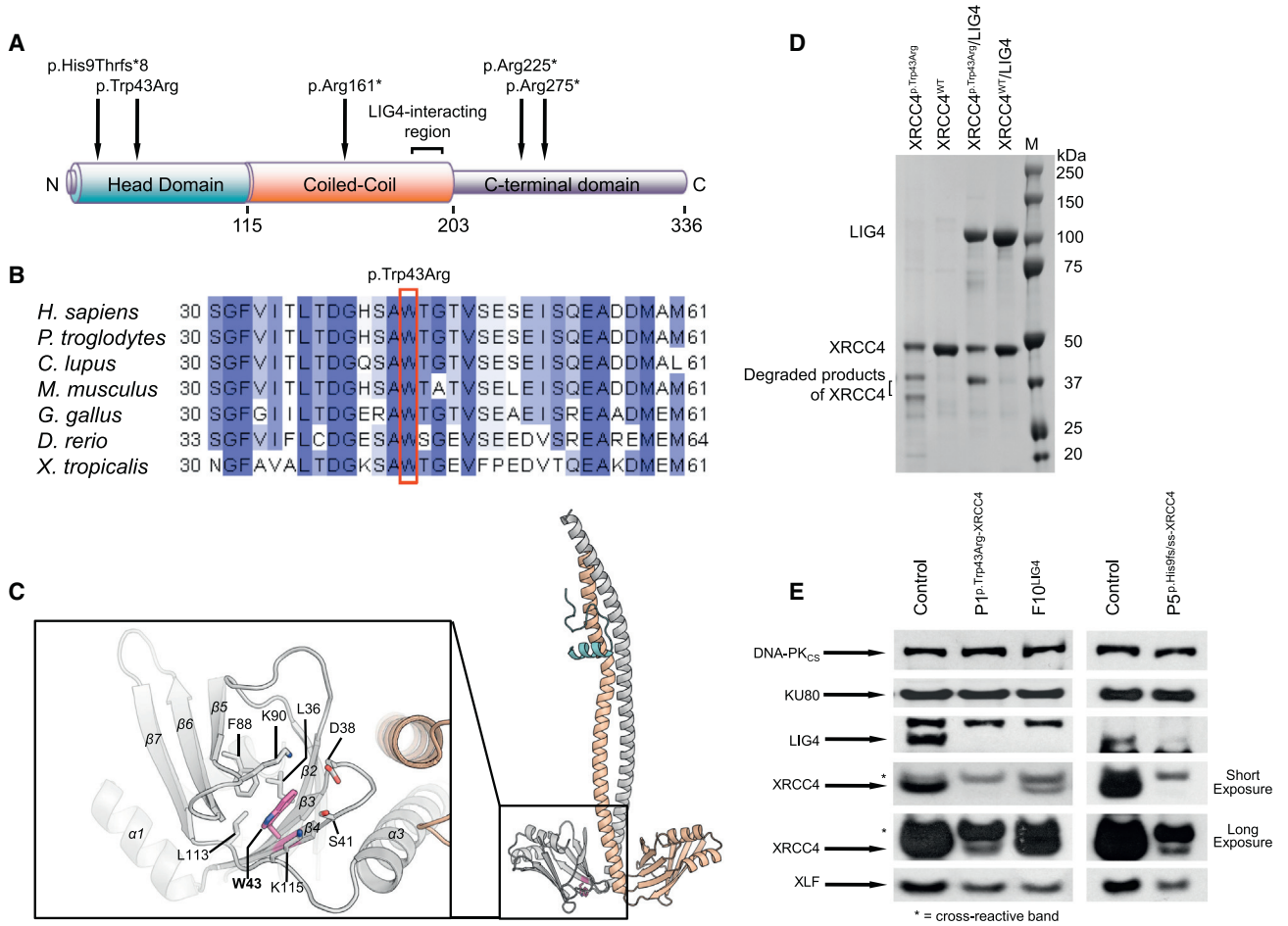

Figure 2. *XRCC4* Mutations Markedly Reduce Levels of Both LIG4 and XRCC4 Proteins
(A) Schematic of XRCC4 indicating protein domains, the LIG4 interaction region, and locations of mutations identified. Head domain, blue; coiled-coiled domain, orange; C-terminal domain, gray.
(B–D) The p.Trp43Arg substitution destabilizes the head domain, significantly reducing XRCC4 stability and solubility.
(B) The tryptophan residue at codon 43 is conserved in all vertebrates. NCBI RefSeq sequences aligned with ClustalOmega.
(C) Trp43 (W43) along with Leu36, Asp38, Ser41, Peh88, Lys90, Leu113, and Lys115 form the hydrophobic core of the head domain of XRCC4. The arginine substitution for tryptophan at codon 43 is likely to distort two layers of β sheets, disrupting the buried hydrophobic core, resulting in exposure of hydrophobic residues to solvent and leading to insolubility, aggregation, and structure destabilization. Left, a magnified view of the head domain containing Trp43. Right, the XRCC4 dimer (silver and gold) in complex with a fragment of LIG4 (cyan) (PDB code 1IK9[39]).
(D) Generation of recombinant XRCC4$^{p.Trp43Arg}$ is substantially less efficient than XRCC4^{WT} protein. Yield of recombinant XRCC4$^{p.Trp3Arg}$ is also reduced even when expressed with its constitutive heterodimer partner LIG4. SDS-PAGE of recombinant LIG4, XRCC4^{WT}, and XRCC4$^{p.Trp43Arg}$, after purification with additional lower-molecular-weight bands consistent with reduced protein stability. Column labeled "M" indicates protein size standards. In contrast to XRCC4^{WT} protein, the majority of XRCC4$^{p.Trp43Arg}$ is insoluble (data not shown).
(E) Both missense and truncating mutations in *XRCC4* markedly reduce both XRCC4 and LIG4 protein levels. Immunoblotting of NHEJ components in control, LIG4, and XRCC4 cells demonstrates that XRCC4 protein is detectable in P1- and P5-derived fibroblasts only after prolonged immunoblot exposure. Because XRCC4 and LIG4 form a stable heterodimer, there is consequential reduction in LIG4 protein levels.

lethality of the mouse *Xrcc4*$^{-/-}$ model[52] supports our conclusion from this and our cellular analyses, that the *XRCC4* mutations represent severe hypomorphic alleles.

Discussion

Our recent description of mutations in *LIG4* as a common cause of MPD prompted us to investigate the relevance of other NHEJ components for the etiology of MPD. Through exome sequencing and next-generation resequencing we have identified six individuals with biallelic mutations in *XRCC4*. We provide comprehensive biochemical, cellular, and immunological analysis to support the pathogenicity of these mutations. In doing so, we also provide functional evidence confirming the deleterious nature of a previously proposed potential pathogenic variant (p.Trp43Arg),[32] which is identical to the mutation we identified in P1. Notably, both individuals, though apparently unrelated, are from Saudi Arabia and therefore the nucleotide

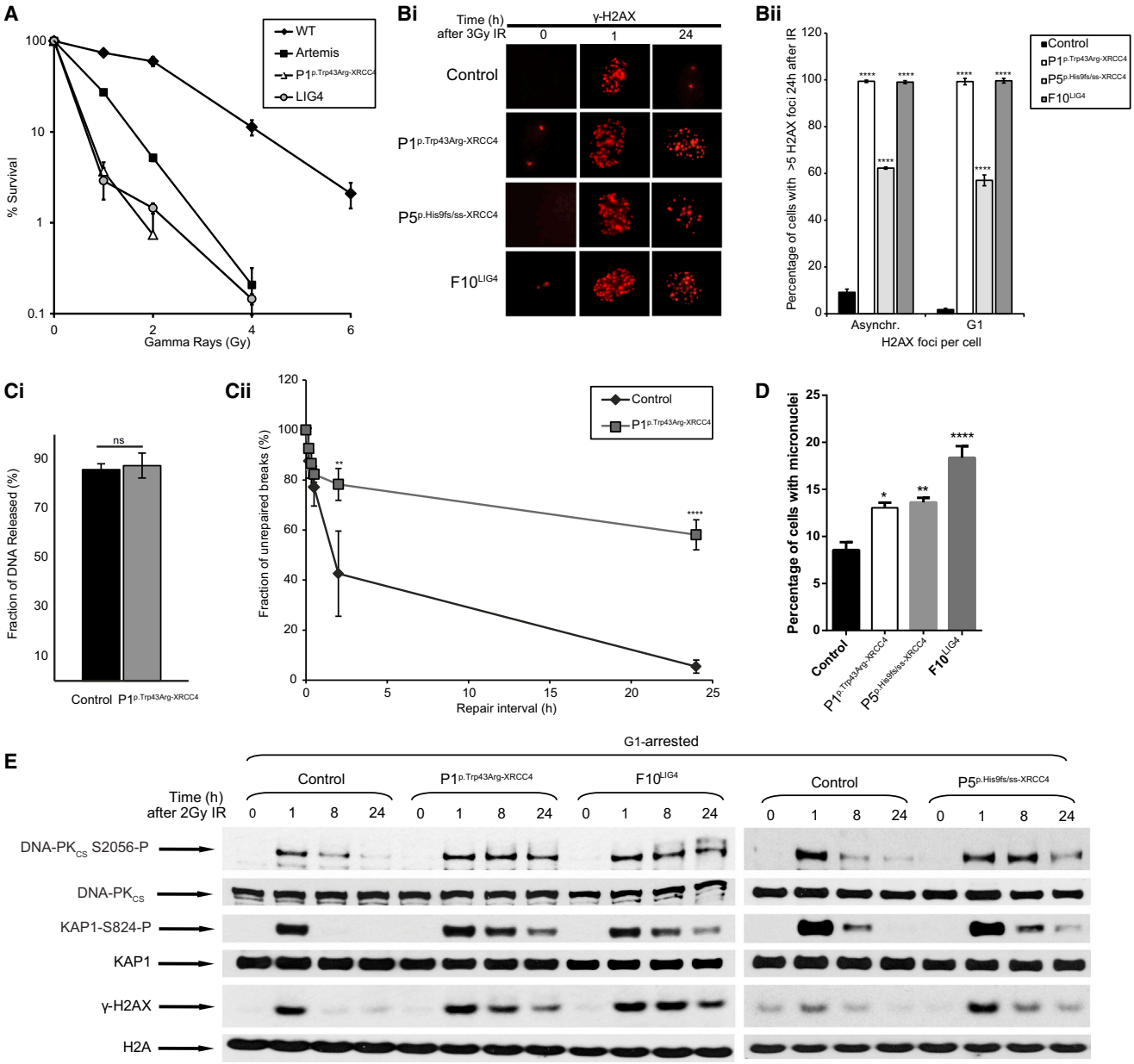

Figure 3. XRCC4 Cells Are Hypersensitive to Ionizing Radiation due to Impaired NHEJ

(A) XRCC4 cells exhibit hypersensitivity to ionizing radiation, similar to LIG4- and Artemis-altered individuals. Clonogenic survival assays performed on primary fibroblasts. Survival at 12–14 days after exposure to ionizing radiation, at doses as indicated. n = 2 experiments. Mean ± SD.

(B) Significantly elevated levels of γ-H2AX foci (a marker of double-strand break formation) are present 24 hr after irradiation in XRCC4 fibroblasts, both in asynchronous (exposed to 3 Gy IR) and G1-arrested cells (exposed to 2 Gy IR). (Bi) Representative immunofluorescence images. Red, γ-H2AX. (Bii) Quantification of γ-H2AX foci. n = 3 experiments. Mean ± SEM. Statistical test: ANOVA. For detailed quantification and time course, see Figures S5 and S6.

(C) Pulse-field gel electrophoresis also demonstrates impaired double-strand DNA break (DSB) resolution in XRCC4 cells after 2.9 Gy IR. Although ionizing radiation results in comparable levels of DSBs in both control and P1 fibroblasts ($XRCC4^{Trp43Arg}$) (Ci), the subsequent kinetics of DSB repair are markedly impaired (Cii). Whereas control cells are able to resolve the majority of breaks within 24 hr, 58% ± 6.0% of breaks remain unresolved in $XRCC4^{p.Trp43Arg}$ cells, compared to 5.4% ± 2.6% in control cells. n = 5 experiments, mean ± SD.

(D) Micronuclei, as indicator of genome instability, was quantified in cells 24 hr after 3 Gy IR. n = 3 experiments, mean ± SEM. Statistical test: ANOVA.

(E) DNA damage response is prolonged in XRCC4 fibroblasts. Immunoblotting of protein extracts from fibroblast cell lines previously synchronized in G1 (to enrich for NHEJ-mediated repair) at time points indicated after 2 Gy IR. Cellular DNA damage response examined by assessing levels of activated H2A (γ-H2AX) and Ser824 phosphorylation of KAP1. The level of NHEJ activity was measured with phosphorylated DNA-PK_{CS}. H2A and KAP1 serve as loading controls.

Table 3. Clinical Hematology and Immunology Characterization of Individuals with XRCC4 Alterations

Pt	Age at Analysis	Hb (g/dl)	WCC (10^3/μl)	Neut	Lymph	Mono	Plts (10^3/μl)	Lymphocyte Subset (cells/μl) (normal range)			Total Ig	IgM (mg/dl)	IgG (mg/dl)	IgA (mg/dl)
								CD3	CD8	CD4	CD19			
P1	5 years	12.0 (11–15)	3.95* (4.3–11.3)	2.02 (1.35–7.5)	1.3* (1.9–4.9)	0.59 (0.25–1)	181 (155–435)	110* (160–270)	47* (60–100)	47* (100–170)	16* (40–80)	NA	NA	1,165	NA
P2	4 years 2 months	12.7 (10.5–13.5)	4.8 (4.7–13.5)	1.7 (1.5–8.5)	2.4 (1.0–5.5)	0.7 (0.1–1.0)	283 (150–450)	133 (90–450)	34 (30–160)	93 (50–240)	28 (20–210)	957	122	701	134
P3-1	11 years 10 months	13.9 (11.5–15.5)	4.5* (5–14)	2.07[a]	1.80[a]	0.43[a]	187 (150–450)	123 (120–260)	50 (37–110)	72 (65–150)	37 (27–86)	1,295	123 (40–230)	1,050 (700–1,500)	122 (70–400)
P3-2	4 years	12.1 (11.5–13.5)	7.44 (6–16)	1.91[a]	4.58[a]	0.6[a]	271 (150–450)	282 (140–370)	119 (49–130)	161 (70–220)	133 (39–140)	987	121 (40–230)	816 (500–1,400)	50 (45–200)
P4	9 years	11.7 (11.5–13.5)	11.5 (5.5–15.5)	5.1 (1.8–8)	4.0 (1.5–6.5)	0.8 (0.2–1)	400 (175–420)	NA	NA	NA	NA	1,281	77 (53–162)	771 (655–1,200)	433 (50–203)
P5	2 years 5 months	12 (10.5–13.5)	12 (5–15)	6.31 (1.5–8.5)	3.44 (2–9.5)	1.19 (0.3–1.5)	570 (150–450)	82%[a]	33%[a]	44%[a]	9%[a]	1,101	87 (50–220)	920 (310–1,380)	94 (30–120)

Reference ranges differ between testing laboratories, so are indicated per individual, where available. Asterisk (*) indicates values below reference range.
[a]Reported as normal by testing laboratory.

substitution probably represents a founder mutation in this population.

All XRCC4-MPD-affected individuals demonstrated in utero and postnatal growth retardation similar to that seen in LIG4-MPD-affected individuals.[14] Microcephaly was present at birth, becoming more evident postnatally. This disproportionate extreme microcephaly suggests that neurogenesis might be particularly sensitive to DNA damage in these individuals, similar to mutations in several other NHEJ genes.[27] Increased apoptosis, reported in the *Xrcc4*$^{-/-}$ mouse,[52] might therefore deplete cell numbers during development, explaining severe reduction in both head size and body size. Failure to resolve DSBs in a timely manner could also slow proliferation, reducing total cell number.

XRCC4 cells exhibit a marked sensitivity to ionizing radiation and therefore clinical exposure to X-rays should be minimized. Although no tumors or hematological malignancy have been observed, our cohort is relatively young in age and given their cellular sensitivity to ionizing radiation and the reports of cancer associated with other NHEJ genes,[53] risks are probably elevated in these individuals. Surprisingly, immune function is preserved in our cohort, despite the key role NHEJ plays in V(D)J recombination to generate adaptive immune cell diversity. Notably, at the molecular level, deficits in specific aspects of recombination are evident, particularly in TdT-dependent random nucleotide insertion. Significantly, this observation provides in vivo validation for previous work demonstrating the role of XRCC4 in recruitment of TdT during V(D)J recombination.[51]

Despite encoding components of a protein complex,[36] *LIG4*- and *XRCC4*-mutated individuals might have phenotypic differences. Individuals with *LIG4* mutations develop pancytopenia, caused by progressive depletion of the hematopoietic stem cell pool.[54] In contrast, *XRCC4*-mutated individuals of a similar age do not demonstrate pancytopenia, suggesting a potential differential requirement for stem cell maintenance. Nevertheless, hematological monitoring of *XRCC4*-mutated individuals should continue because pancytopenia could develop in later childhood. The identification of older individuals would also help address this specific issue. Furthermore, resequencing of *XRCC4* in individuals with RS-SCID and other cohorts will be important to define the full spectrum of phenotypes associated with mutations in this gene.

Severe growth failure without symptomatic immunodeficiency in many *LIG4*- and *XRCC4*-mutated individuals suggests a phenotype spectrum among individuals with NHEJ mutations (Figure S7). At one end, mutations cause extreme growth failure and microcephaly, whereas conversely, mutations in *DCLRE1C* (encoding Artemis) cause RS-SCID (radiosensitive severe combined immunodeficiency) without microcephaly or short stature.[27] With *NHEJ1* (encoding XLF) mutations, RS-SCID is typically seen in conjunction with marked microcephaly and growth failure (MIM 611291).[30]

A

	Unique productive *IGH* sequences	Total number of N nucleotides	Total number of nucleotide deletions	Total number of P nucleotides
Control	4363	12.44	17.19	0.59
Control	4822	12.71	17.70	0.54
P1	5889	7.35	15.38	0.68
P2	1912	7.51	17.21	0.52
P3-1	1715	8.82	18.38	0.46
P3-2	2995	8.14	17.91	0.50

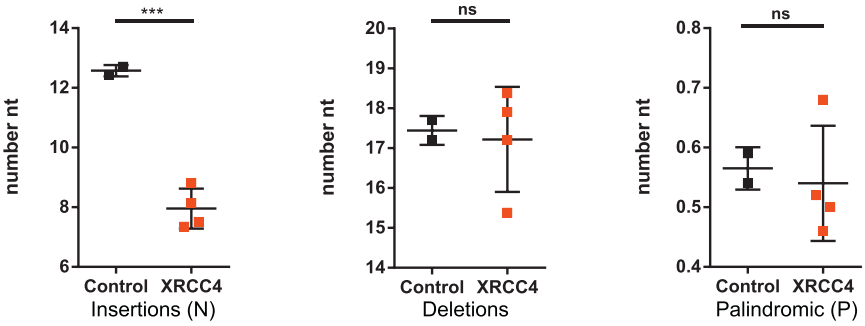

B

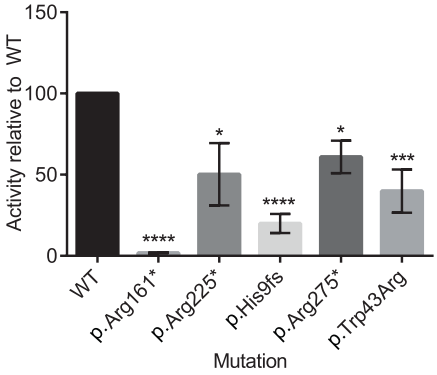

Figure 4. *XRCC4* Mutations Do Not Significantly Impact V(D)J Recombination
(A) Next-generation sequencing of the recombined IgH locus demonstrates that XRCC4 lymphocytes contain a large number of unique V(D)J recombination events. Upper panel, summary of V(D)J junction characteristics following 454 deep sequencing and analysis using the IGGalaxy antigen receptor tool. Lower panel, a significant decrease in insertional events is detected at V(D)J junctions ($p = 0.0008$; t test), providing in vivo confirmation for XRCC4's role in recruiting terminal deoxynucleotide transferase to immunoglobulin V(D)J junctions, which adds additional nucleotides during recombination. Mean ± SD.
(B) Missense and some truncated forms of XRCC4 retain reduced competence for V(D)J recombination. Plasmids of *XRCC4* cDNA with mutations (as indicated) were overexpressed in an XRCC4-deficient cell line and recombination activity assayed by qRT-PCR. Efficiency is expressed as percentage of wild-type activity. $n = 4$ experiments, error bars = SEM. *$p < 0.05$; ***$p < 0.001$; ****$p < 0.0001$.

Such variation in phenotypes between individuals with mutations in NHEJ genes poses an important question as to the respective role of the proteins they encode in adaptive immunity, neurogenesis, and general growth. *XRCC4* mutations are likely to result in a global reduction in efficiency of NHEJ repair during development, explaining reduced body size and microcephaly. Residual ligase complex activity in these individuals could, however, explain the absence of SCID phenotype, because positive selection of cells possessing functional T cell receptors and immunoglobulins during adaptive immune cell maturation might be able to compensate for impaired V(D)J recombination efficiency. In contrast, null mutations in *DCLRE1C* (encoding Artemis) cause RS-SCID with no microcephaly or growth deficit (MIM 602450),[27] because only a subset of DSBs arising from DNA damage require Artemis[55] and therefore NHEJ repair during development might be sufficient for normal growth. However, in order for V(D)J recombination to succeed, additional end-processing by Artemis is essential to cleave hairpin structures formed after the actions of RAG1/2.[56] Failure to perform this cleavage consequently causes the RS-SCID phenotype.

Although microcephaly and growth failure in both *LIG4*- and *XLF*-mutated individuals might be attributed to their core role in NHEJ ligation, why XLF, in contrast to LIG4 and XRCC4, has invariably been associated with SCID is less easy to explain. Likewise, gene-phenotype correlations are complicated by striking variation between individuals with mutations in *PRKDC* (encoding DNA-PK_{CS} [MIM 615966]) and also in *LIG4*.[22,28,29] Additional complexities in NHEJ mechanisms, including regulatory phosphorylation by DNA-PK_{CS} on multiple components,[57] functional redundancy,[58] and alternative cellular pathways[59] might help account for these differences.

In summary, we present comprehensive genetic and cellular evidence that mutations in *XRCC4* cause microcephalic primordial dwarfism. The absence of an overt clinical immunodeficiency highlights differing requirements for NHEJ genes during growth, neurogenesis, and generation of the adaptive immune repertoire, demonstrating the complexity of this important cellular pathway.

Supplemental Data

Supplemental Data include seven figures and four tables and can be found with this article online at http://dx.doi.org/10.1016/j.ajhg.2015.01.013.

Acknowledgments

The authors thank the individuals and their families for their involvement and cooperation in this research; S. Brown and A. Gallagher and the MRC HGU sequencing core for technical support; M. McDonald and K. Mackenzie for helpful discussions; and Dr. Katherine Stott for her assistance with the CD experiment and data analysis. Ion Proton sequencing was performed by the Wellcome Trust Clinical Research Facility, Western General Hospital, Edinburgh. The authors acknowledge the Exome Aggregation Consortium and the groups therein for providing control exome variant data. A full list of contributing groups to ExAC can be found online (http://exac.broadinstitute.org/about). L.S.B. is funded by Medical Research Scotland. P.C. is funded by Newlife Foundation for Disabled Children. A.P.J. is funded by the MRC (U127580972) and ERC (HumGensize 281847). G.S.S. and A.P.J. are Lister Institute for Preventative Medicine Fellows. G.S.S. is funded by a CR-UK Senior Fellowship (C17183/A13030). M.v.d.B. and H.IJ. are supported by a Vidi grant of ZonMW (91712323). B.K. has been funded by MRC CiC and BWHRF (P/O 088314). T.O., Q.W., and T.L.B. are funded by Wellcome Trust.

Received: December 18, 2014
Accepted: January 16, 2015
Published: February 26, 2015

Web Resources

The URLs for data presented herein are as follows:

ExAC Browser, http://exac.broadinstitute.org/
OMIM, http://www.omim.org/
RefSeq, http://www.ncbi.nlm.nih.gov/RefSeq

References

1. Klingseisen, A., and Jackson, A.P. (2011). Mechanisms and pathways of growth failure in primordial dwarfism. Genes Dev. *25*, 2011–2024.
2. Willems, M., Geneviève, D., Borck, G., Baumann, C., Baujat, G., Bieth, E., Edery, P., Farra, C., Gerard, M., Héron, D., et al. (2010). Molecular analysis of pericentrin gene (PCNT) in a series of 24 Seckel/microcephalic osteodysplastic primordial dwarfism type II (MOPD II) families. J. Med. Genet. *47*, 797–802.
3. Edery, P., Marcaillou, C., Sahbatou, M., Labalme, A., Chastang, J., Touraine, R., Tubacher, E., Senni, F., Bober, M.B., Nampoothiri, S., et al. (2011). Association of TALS developmental disorder with defect in minor splicing component U4atac snRNA. Science *332*, 240–243.
4. He, H., Liyanarachchi, S., Akagi, K., Nagy, R., Li, J., Dietrich, R.C., Li, W., Sebastian, N., Wen, B., Xin, B., et al. (2011). Mutations in U4atac snRNA, a component of the minor spliceosome, in the developmental disorder MOPD I. Science *332*, 238–240.
5. Griffith, E., Walker, S., Martin, C.A., Vagnarelli, P., Stiff, T., Vernay, B., Al Sanna, N., Saggar, A., Hamel, B., Earnshaw, W.C., et al. (2008). Mutations in pericentrin cause Seckel syndrome with defective ATR-dependent DNA damage signaling. Nat. Genet. *40*, 232–236.
6. Rauch, A., Thiel, C.T., Schindler, D., Wick, U., Crow, Y.J., Ekici, A.B., van Essen, A.J., Goecke, T.O., Al-Gazali, L., Chrzanowska, K.H., et al. (2008). Mutations in the pericentrin (PCNT) gene cause primordial dwarfism. Science *319*, 816–819.
7. Bicknell, L.S., Bongers, E.M., Leitch, A., Brown, S., Schoots, J., Harley, M.E., Aftimos, S., Al-Aama, J.Y., Bober, M., Brown, P.A., et al. (2011). Mutations in the pre-replication complex cause Meier-Gorlin syndrome. Nat. Genet. *43*, 356–359.
8. Bicknell, L.S., Walker, S., Klingseisen, A., Stiff, T., Leitch, A., Kerzendorfer, C., Martin, C.A., Yeyati, P., Al Sanna, N., Bober, M., et al. (2011). Mutations in ORC1, encoding the largest subunit of the origin recognition complex, cause microcephalic primordial dwarfism resembling Meier-Gorlin syndrome. Nat. Genet. *43*, 350–355.
9. Guernsey, D.L., Matsuoka, M., Jiang, H., Evans, S., Macgillivray, C., Nightingale, M., Perry, S., Ferguson, M., LeBlanc, M., Paquette, J., et al. (2011). Mutations in origin recognition complex gene ORC4 cause Meier-Gorlin syndrome. Nat. Genet. *43*, 360–364.
10. O'Driscoll, M., Ruiz-Perez, V.L., Woods, C.G., Jeggo, P.A., and Goodship, J.A. (2003). A splicing mutation affecting expression of ataxia-telangiectasia and Rad3-related protein (ATR) results in Seckel syndrome. Nat. Genet. *33*, 497–501.
11. Ogi, T., Walker, S., Stiff, T., Hobson, E., Limsirichaikul, S., Carpenter, G., Prescott, K., Suri, M., Byrd, P.J., Matsuse, M., et al. (2012). Identification of the first ATRIP-deficient patient and novel mutations in ATR define a clinical spectrum for ATR-ATRIP Seckel Syndrome. PLoS Genet. *8*, e1002945.
12. Qvist, P., Huertas, P., Jimeno, S., Nyegaard, M., Hassan, M.J., Jackson, S.P., and Børglum, A.D. (2011). CtIP mutations cause Seckel and Jawad Syndromes. PLoS Genet. *7*, e1002310.
13. IJspeert, H., Warris, A., van der Flier, M., Reisli, I., Keles, S., Chishimba, S., van Dongen, J.J., van Gent, D.C., and van der Burg, M. (2013). Clinical spectrum of LIG4 deficiency is broadened with severe dysmaturity, primordial dwarfism, and neurological abnormalities. Hum. Mutat. *34*, 1611–1614.
14. Murray, J.E., Bicknell, L.S., Yigit, G., Duker, A.L., van Kogelenberg, M., Haghayegh, S., Wieczorek, D., Kayserili, H., Albert, M.H., Wise, C.A., et al. (2014). Extreme growth failure is a common presentation of ligase IV deficiency. Hum. Mutat. *35*, 76–85.
15. Stewart, D.R., Pemov, A., Johnston, J.J., Sapp, J.C., Yeager, M., He, J., Boland, J.F., Burdett, L., Brown, C., Gatti, R.A., et al. (2014). Dubowitz syndrome is a complex comprised of multiple, genetically distinct and phenotypically overlapping disorders. PLoS ONE *9*, e98686.
16. Ben-Omran, T.I., Cerosaletti, K., Concannon, P., Weitzman, S., and Nezarati, M.M. (2005). A patient with mutations in DNA Ligase IV: clinical features and overlap with Nijmegen breakage syndrome. Am. J. Med. Genet. A. *137A*, 283–287.
17. Buck, D., Moshous, D., de Chasseval, R., Ma, Y., le Deist, F., Cavazzana-Calvo, M., Fischer, A., Casanova, J.L., Lieber, M.R., and de Villartay, J.P. (2006). Severe combined immunodeficiency and microcephaly in siblings with hypomorphic mutations in DNA ligase IV. Eur. J. Immunol. *36*, 224–235.
18. Gruhn, B., Seidel, J., Zintl, F., Varon, R., Tönnies, H., Neitzel, H., Bechtold, A., Hoehn, H., and Schindler, D. (2007). Successful bone marrow transplantation in a patient with DNA ligase IV deficiency and bone marrow failure. Orphanet J. Rare Dis. *2*, 5.
19. O'Driscoll, M., Cerosaletti, K.M., Girard, P.M., Dai, Y., Stumm, M., Kysela, B., Hirsch, B., Gennery, A., Palmer, S.E., Seidel, J., et al. (2001). DNA ligase IV mutations identified in patients

exhibiting developmental delay and immunodeficiency. Mol. Cell *8*, 1175–1185.
20. Plowman, P.N., Bridges, B.A., Arlett, C.F., Hinney, A., and Kingston, J.E. (1990). An instance of clinical radiation morbidity and cellular radiosensitivity, not associated with ataxia-telangiectasia. Br. J. Radiol. *63*, 624–628.
21. Riballo, E., Critchlow, S.E., Teo, S.H., Doherty, A.J., Priestley, A., Broughton, B., Kysela, B., Beamish, H., Plowman, N., Arlett, C.F., et al. (1999). Identification of a defect in DNA ligase IV in a radiosensitive leukaemia patient. Curr. Biol. *9*, 699–702.
22. van der Burg, M., van Veelen, L.R., Verkaik, N.S., Wiegant, W.W., Hartwig, N.G., Barendregt, B.H., Brugmans, L., Raams, A., Jaspers, N.G., Zdzienicka, M.Z., et al. (2006). A new type of radiosensitive T-B-NK+ severe combined immunodeficiency caused by a LIG4 mutation. J. Clin. Invest. *116*, 137–145.
23. Chiruvella, K.K., Liang, Z., and Wilson, T.E. (2013). Repair of double-strand breaks by end joining. Cold Spring Harb. Perspect. Biol. *5*, a012757.
24. Deriano, L., and Roth, D.B. (2013). Modernizing the nonhomologous end-joining repertoire: alternative and classical NHEJ share the stage. Annu. Rev. Genet. *47*, 433–455.
25. Wu, Q., Ochi, T., Matak-Vinkovic, D., Robinson, C.V., Chirgadze, D.Y., and Blundell, T.L. (2011). Non-homologous end-joining partners in a helical dance: structural studies of XLF-XRCC4 interactions. Biochem. Soc. Trans. *39*, 1387–1392, 2, 1392.
26. Malu, S., Malshetty, V., Francis, D., and Cortes, P. (2012). Role of non-homologous end joining in V(D)J recombination. Immunol. Res. *54*, 233–246.
27. Woodbine, L., Gennery, A.R., and Jeggo, P.A. (2014). The clinical impact of deficiency in DNA non-homologous end-joining. DNA Repair (Amst.) *16*, 84–96.
28. van der Burg, M., Ijspeert, H., Verkaik, N.S., Turul, T., Wiegant, W.W., Morotomi-Yano, K., Mari, P.O., Tezcan, I., Chen, D.J., Zdzienicka, M.Z., et al. (2009). A DNA-PKcs mutation in a radiosensitive T-B- SCID patient inhibits Artemis activation and nonhomologous end-joining. J. Clin. Invest. *119*, 91–98.
29. Woodbine, L., Neal, J.A., Sasi, N.K., Shimada, M., Deem, K., Coleman, H., Dobyns, W.B., Ogi, T., Meek, K., Davies, E.G., and Jeggo, P.A. (2013). PRKDC mutations in a SCID patient with profound neurological abnormalities. J. Clin. Invest. *123*, 2969–2980.
30. Buck, D., Malivert, L., de Chasseval, R., Barraud, A., Fondanèche, M.C., Sanal, O., Plebani, A., Stéphan, J.L., Hufnagel, M., le Deist, F., et al. (2006). Cernunnos, a novel nonhomologous end-joining factor, is mutated in human immunodeficiency with microcephaly. Cell *124*, 287–299.
31. Dutrannoy, V., Demuth, I., Baumann, U., Schindler, D., Konrat, K., Neitzel, H., Gillessen-Kaesbach, G., Radszewski, J., Rothe, S., Schellenberger, M.T., et al. (2010). Clinical variability and novel mutations in the NHEJ1 gene in patients with a Nijmegen breakage syndrome-like phenotype. Hum. Mutat. *31*, 1059–1068.
32. Shaheen, R., Faqeih, E., Ansari, S., Abdel-Salam, G., Al-Hassnan, Z.N., Al-Shidi, T., Alomar, R., Sogaty, S., and Alkuraya, F.S. (2014). Genomic analysis of primordial dwarfism reveals novel disease genes. Genome Res. *24*, 291–299.
33. Cole, T.J., Freeman, J.V., and Preece, M.A. (1998). British 1990 growth reference centiles for weight, height, body mass index and head circumference fitted by maximum penalized likelihood. Stat. Med. *17*, 407–429.
34. Martin, C.A., Ahmad, I., Klingseisen, A., Hussain, M.S., Bicknell, L.S., Leitch, A., Nürnberg, G., Toliat, M.R., Murray, J.E., Hunt, D., et al. (2014). Mutations in PLK4, encoding a master regulator of centriole biogenesis, cause microcephaly, growth failure and retinopathy. Nat. Genet. *46*, 1283–1292.
35. Robinson, J.T., Thorvaldsdóttir, H., Winckler, W., Guttman, M., Lander, E.S., Getz, G., and Mesirov, J.P. (2011). Integrative genomics viewer. Nat. Biotechnol. *29*, 24–26.
36. Critchlow, S.E., Bowater, R.P., and Jackson, S.P. (1997). Mammalian DNA double-strand break repair protein XRCC4 interacts with DNA ligase IV. Curr. Biol. *7*, 588–598.
37. Peränen, J., Rikkonen, M., Hyvönen, M., and Kääriäinen, L. (1996). T7 vectors with modified T7lac promoter for expression of proteins in *Escherichia coli*. Anal. Biochem. *236*, 371–373.
38. Wang, Y., Lamarche, B.J., and Tsai, M.D. (2007). Human DNA ligase IV and the ligase IV/XRCC4 complex: analysis of nick ligation fidelity. Biochemistry *46*, 4962–4976.
39. Sibanda, B.L., Critchlow, S.E., Begun, J., Pei, X.Y., Jackson, S.P., Blundell, T.L., and Pellegrini, L. (2001). Crystal structure of an Xrcc4-DNA ligase IV complex. Nat. Struct. Biol. *8*, 1015–1019.
40. Lee, G.S., Neiditch, M.B., Salus, S.S., and Roth, D.B. (2004). RAG proteins shepherd double-strand breaks to a specific pathway, suppressing error-prone repair, but RAG nicking initiates homologous recombination. Cell *117*, 171–184.
41. Kysela, B.P., Arrand, J.E., and Michael, B.D. (1993). Relative contributions of levels of initial damage and repair of double-strand breaks to the ionizing radiation-sensitive phenotype of the Chinese hamster cell mutant, XR-V15B. Part II. Neutrons. Int. J. Radiat. Biol. *64*, 531–538.
42. van Dongen, J.J., Langerak, A.W., Brüggemann, M., Evans, P.A., Hummel, M., Lavender, F.L., Delabesse, E., Davi, F., Schuuring, E., García-Sanz, R., et al. (2003). Design and standardization of PCR primers and protocols for detection of clonal immunoglobulin and T-cell receptor gene recombinations in suspect lymphoproliferations: report of the BIOMED-2 Concerted Action BMH4-CT98-3936. Leukemia *17*, 2257–2317.
43. Alamyar, E., Duroux, P., Lefranc, M.P., and Giudicelli, V. (2012). IMGT(®) tools for the nucleotide analysis of immunoglobulin (IG) and T cell receptor (TR) V-(D)-J repertoires, polymorphisms, and IG mutations: IMGT/V-QUEST and IMGT/HighV-QUEST for NGS. Methods Mol. Biol. *882*, 569–604.
44. Goecks, J., Nekrutenko, A., and Taylor, J.; Galaxy Team (2010). Galaxy: a comprehensive approach for supporting accessible, reproducible, and transparent computational research in the life sciences. Genome Biol. *11*, R86.
45. Blankenberg, D., Von Kuster, G., Coraor, N., Ananda, G., Lazarus, R., Mangan, M., Nekrutenko, A., and Taylor, J. (2010). Galaxy: a web-based genome analysis tool for experimentalists. Curr. Protoc. Mol. Biol. *Chapter 19*, 1–21.
46. Giardine, B., Riemer, C., Hardison, R.C., Burhans, R., Elnitski, L., Shah, P., Zhang, Y., Blankenberg, D., Albert, I., Taylor, J., et al. (2005). Galaxy: a platform for interactive large-scale genome analysis. Genome Res. *15*, 1451–1455.
47. Team, R.C. (2013). R: A Language and Environment for Statistical Computing (Vienna, Austria: R Foundation for Statistical Computing).
48. Cingolani, P., Platts, A., Wang, L., Coon, M., Nguyen, T., Wang, L., Land, S.J., Lu, X., and Ruden, D.M. (2012). A program for annotating and predicting the effects of single nucleotide polymorphisms, SnpEff: SNPs in the genome of

Drosophila melanogaster strain w1118; iso-2; iso-3. Fly (Austin) *6*, 80–92.
49. Pires, D.E., Ascher, D.B., and Blundell, T.L. (2014). DUET: a server for predicting effects of mutations on protein stability using an integrated computational approach. Nucleic Acids Res. *42*, W314–W319.
50. van der Burg, M., Verkaik, N.S., den Dekker, A.T., Barendregt, B.H., Pico-Knijnenburg, I., Tezcan, I., vanDongen, J.J., and van Gent, D.C. (2007). Defective Artemis nuclease is characterized by coding joints with microhomology in long palindromic-nucleotide stretches. Eur. J. Immunol. *37*, 3522–3528.
51. Boubakour-Azzouz, I., Bertrand, P., Claes, A., Lopez, B.S., and Rougeon, F. (2012). Terminal deoxynucleotidyl transferase requires KU80 and XRCC4 to promote N-addition at non-V(D)J chromosomal breaks in non-lymphoid cells. Nucleic Acids Res. *40*, 8381–8391.
52. Gao, Y., Sun, Y., Frank, K.M., Dikkes, P., Fujiwara, Y., Seidl, K.J., Sekiguchi, J.M., Rathbun, G.A., Swat, W., Wang, J., et al. (1998). A critical role for DNA end-joining proteins in both lymphogenesis and neurogenesis. Cell *95*, 891–902.
53. de Miranda, N.F., Peng, R., Georgiou, K., Wu, C., Falk Sörqvist, E., Berglund, M., Chen, L., Gao, Z., Lagerstedt, K., Lisboa, S., et al. (2013). DNA repair genes are selectively mutated in diffuse large B cell lymphomas. J. Exp. Med. *210*, 1729–1742.
54. Nijnik, A., Woodbine, L., Marchetti, C., Dawson, S., Lambe, T., Liu, C., Rodrigues, N.P., Crockford, T.L., Cabuy, E., Vindigni, A., et al. (2007). DNA repair is limiting for haematopoietic stem cells during ageing. Nature *447*, 686–690.
55. Riballo, E., Kühne, M., Rief, N., Doherty, A., Smith, G.C., Recio, M.J., Reis, C., Dahm, K., Fricke, A., Krempler, A., et al. (2004). A pathway of double-strand break rejoining dependent upon ATM, Artemis, and proteins locating to gamma-H2AX foci. Mol. Cell *16*, 715–724.
56. McBlane, J.F., van Gent, D.C., Ramsden, D.A., Romeo, C., Cuomo, C.A., Gellert, M., and Oettinger, M.A. (1995). Cleavage at a V(D)J recombination signal requires only RAG1 and RAG2 proteins and occurs in two steps. Cell *83*, 387–395.
57. Neal, J.A., and Meek, K. (2011). Choosing the right path: does DNA-PK help make the decision? Mutat. Res. *711*, 73–86.
58. Zha, S., Guo, C., Boboila, C., Oksenych, V., Cheng, H.L., Zhang, Y., Wesemann, D.R., Yuen, G., Patel, H., Goff, P.H., et al. (2011). ATM damage response and XLF repair factor are functionally redundant in joining DNA breaks. Nature *469*, 250–254.
59. McVey, M., and Lee, S.E. (2008). MMEJ repair of double-strand breaks (director's cut): deleted sequences and alternative endings. Trends Genet. *24*, 529–538.